Geophysical Research Letters

RESEARCH LETTER
10.1029/2019GL086075

Key Points:
- AMOC mean strength is well reproduced by the CMIP6 multimodel mean, but large model spread persists
- Projected AMOC decline by the end of the 21st century shows weak dependence on the SSP scenarios
- An emergent constraint between AMOC strength and projected decline suggests possible AMOC decline between 34% and 45% by 2100

Supporting Information:
- Supporting Information S1

Correspondence to:
W. Weijer,
wilbert@lanl.gov

Citation:
Weijer, W., Cheng, W., Garuba, O. A., Hu, A., & Nadiga, B. T. (2020). CMIP6 models predict significant 21st century decline of the Atlantic Meridional Overturning Circulation. *Geophysical Research Letters*, *47*, e2019GL086075. https://doi.org/10.1029/2019GL086075

Received 5 NOV 2019
Accepted 7 MAY 2020
Accepted article online 24 MAY 2020

CMIP6 Models Predict Significant 21st Century Decline of the Atlantic Meridional Overturning Circulation

W. Weijer[1], **W. Cheng**[2,3], **O. A. Garuba**[4], **A. Hu**[5], and **B. T. Nadiga**[1]

[1]Los Alamos National Laboratory, Los Alamos, NM, USA, [2]Joint Institute for the Study of the Atmosphere and Ocean, University of Washington, Seattle, WA, USA, [3]NOAA/Pacific Marine Environmental Laboratory, Seattle, WA, USA, [4]Pacific Northwest National Laboratory, Richland, WA, USA, [5]National Center for Atmospheric Research, Boulder, CO, USA

Abstract We explore the representation of the Atlantic Meridional Overturning Circulation (AMOC) in 27 models from the CMIP6 multimodel ensemble. Comparison with RAPID and SAMBA observations suggests that the ensemble mean represents the AMOC strength and vertical profile reasonably well. Linear trends over the entire historical period (1850–2014) are generally neutral, but many models exhibit an AMOC peak around the 1980s. Ensemble mean AMOC decline in future (SSP) scenarios is stronger in CMIP6 than CMIP5 models. In fact, AMOC decline in CMIP6 is surprisingly insensitive to the scenario at least up to 2060. We find an emergent relationship among a majority of models between AMOC strength and 21st century AMOC decline. Constraining this relationship with RAPID observations suggests that the AMOC might decline between 6 and 8 Sv (34–45%) by 2100. A smaller group of models projects much less AMOC weakening of only up to 30%.

Plain Language Summary The Atlantic Meridional Overturning Circulation (AMOC) is a circulation pattern in the Atlantic Ocean that is an important component of the climate system, due to its ability to redistribute and sequester heat and carbon. An accurate representation of the AMOC is a critical test for climate models and essential for building confidence in their projections. Here we investigate the AMOC in 27 climate models that contributed simulations to the Coupled Model Intercomparison Project Phase 6 (CMIP6). We find that many models reproduce the observed AMOC quite well, but there are still several models in which the AMOC is too weak or too strong. Most models suggest a slight upward trend in the AMOC from 1850 to the 1980s. Simulations representing different scenarios for future socioeconomic development suggest a stronger AMOC decline compared to previous assessments. Using direct measurements of the AMOC since 2004 and an emerging across-model relationship between AMOC decline in the 21st century and their present-day mean state, we find that the majority of CMIP6 models point to an end of century AMOC weakening of 34–45% of its present-day strength. A smaller group of models projects much less weakening of only up to 30% of its present state.

1. Introduction

The Atlantic Meridional Overturning Circulation (AMOC) is an important regulator of the climate system. It plays a key role in the global redistribution of heat, as it accounts for roughly 2/3 of the oceanic northward heat transport at northern midlatitudes (Johns et al., 2011; Trenberth et al., 2019) and is responsible for net *equatorward* ocean heat transport in the South Atlantic (estimated to be of the order of 0.5 PW Dong et al., 2009; Trenberth et al., 2019), a unique feature among ocean basins. Not only does the AMOC influence the subpolar North Atlantic (e.g., Palter, 2015) but its impacts include the position of the Intertropical Convergence Zone (ITCZ; e.g., Marshall et al., 2014); Arctic sea ice (e.g., Day et al., 2012; Mahajan et al., 2011; Yeager & Robson, 2017); and the global response to Arctic sea ice loss (e.g., Tomas et al., 2016). The AMOC is also a significant driver of carbon (e.g., Carlson et al., 2010; Fontela et al., 2016) and heat (e.g., Häkkinen et al., 2015; Kostov et al., 2014) sequestration in the subsurface ocean. Clearly, the response of the AMOC to continued anthropogenic forcing will strongly determine the trajectory of Earth's climate in the 21st century and beyond.

An accurate representation of the mean state, variability, and sensitivity to anthropogenic forcing of AMOC is a critical test for climate models and is essential for building confidence in the projections they produce. The various phases of the Coupled Model Intercomparison Project (CMIP) have given us an excellent

opportunity to assess the evolution of AMOC representation through consecutive generations of models. Coordinated by the World Climate Research Programme (WCRP), CMIP specifies a set of experimental protocols that enables modeling centers to run identical experiments with their models. Analyzing the resulting ensemble of simulations allows us to explore the robustness of—or uncertainties in—the simulated climate behavior. Studies like Weaver et al. (2012) and Cheng et al. (2013) showed a wide range of AMOC behaviors in models participating in Phase 5 of CMIP (CMIP5). Phase 6 (CMIP6 Eyring et al., 2016) will give us an opportunity to evaluate AMOC behavior in the new generation of climate models.

But there is another factor that makes it timely to revisit the AMOC in climate models. Until about a decade ago, direct observations of the AMOC were limited to sparse trans-Atlantic hydrographic surveys (e.g., Bryden et al., 2005), and validation of the AMOC in models was ad hoc at best. During the last decade and a half, however, several observational programs have been systematically monitoring the AMOC across the Atlantic basin (Frajka-Williams et al., 2019). The most comprehensive effort to date is the the Rapid Climate Change-Meridional Overturning Circulation and Heatflux Array (RAPID/MOCHA), which has been continuously monitoring the AMOC at 26°N since April 2004. Currently, more than 14 years of data are available, indicating a mean AMOC strength of 17.7 ± 0.3 Sv (Smeed et al., 2019). A similar effort in the South Atlantic (the South Atlantic MOC Basin-wide Array, or SAMBA) estimates the mean AMOC at 34°S to be 14.6 Sv (Frajka-Williams et al., 2019). A cross-Atlantic observational program in the subpolar North Atlantic (Overturning in the Subpolar North Atlantic Program, or OSNAP) has provided a first glimpse of the overturning in the Labrador Sea (OSNAP West; 2.1 ± 0.3 Sv) and between Greenland and Scotland (OSNAP East; 15.6 ± 0.8 Sv Lozier et al., 2019).

These observations provide useful reference values for evaluating the representation of the AMOC in models. Furthermore, we will examine whether the multimodel data exhibit any "emergent constraint" relationships (Hall et al., 2019), in particular, whether the modeled future decline of the AMOC in the 21st century is related to their historical mean states as suggested by previous generation CMIP models (Gregory et al., 2005; Weaver et al., 2012). Such a relationship would allow us to calibrate the AMOC decline in the 21st century using the present-day observations, thus providing a best-guess quantification of the AMOC strength into the future.

2. Method

2.1. CMIP6 Models Used in This Analysis

We analyze CMIP historical simulations (Eyring et al., 2016) and four scenarios from the Scenario Model Intercomparison Project (ScenarioMIP; O'Neill et al., 2016). The protocol for the historical simulations (experiment name: "historical") calls for 165-year simulations (from 1850 to 2014), with forcing fields that are based on observations whenever possible (Hoesly et al., 2018; Meinshausen et al., 2017). The scenario simulations are run for 86 years, from 2015 to 2100. ScenarioMIP recommends four tier-1 simulation protocols, reflecting different Shared Socioeconomic Pathways (SSPs) that result in different radiative forcing magnitudes by 2100. These experiments represent low-end (SSP1-2.6: "ssp126"), medium-end (SSP2-4.5: "ssp245"), and high-end (SSP3-7.0: "ssp370"; SSP5-8.5: "ssp585") forcing scenarios. We also use $4xCO_2$ ("abrupt4xCO2") simulations and historical simulations in which only the greenhouse gas concentrations ("hist_GHG") or aerosols ("hist_aer") were varied.

We use output from 27 different models, as listed in Table 1 and Tables S1 and S2 in the supporting information. These models had submitted the stream function variable (msftmz and msftyz) for the historical simulations to the ESGF archive by the time of our data freeze (15 January 2020). Eighteen models contributed SSP simulations, four of which contributed only a subset of the tier-1 simulations.

We define AMOC strength as the maximum of the overturning stream function in the Atlantic Ocean and evaluate AMOC characteristics at 26°N and 34°S. The term "historical period" is understood to be the 1850–2014 period of the CMIP6 historical simulations, while the "RAPID period" is defined here as the 2005–2014 period of overlap between the historical period and the years for which full year's worth of RAPID data is available (2005–2017).

In this paper we use standard error of the mean σ_μ to quantify the uncertainty in the estimation of the mean μ based on a limited number of samples (ensemble members or time series points). It is defined as $\sigma/\sqrt{n}$,

Geophysical Research Letters

10.1029/2019GL086075

Table 1
The Models Analyzed in This Study, the Modeling Centers That Contributed Them, a Key Reference, and Citations to the Data Sets Used

Model	Modeling center	Key reference	Data citations
ACCESS-CM2	CSIRO-ARCCSS	Bi et al. (2013)[a]	Dix et al. (2019a, 2019b, 2019c, 2019d, 2019e, 2019f)
ACCESS-ESM1-5	CSIRO	Law et al. (2017); Ziehn et al. (2017)	Ziehn et al. (2019a, 2019b, 2019c, 2019d, 2019e, 2019f)
CanESM5	CCCma	Swart et al. (2019a)	Swart et al. (2019b, 2019c, 2019d, 2019e, 2019f, 2019g)
CESM2	NCAR	Danabasoglu et al. (2020)	Danabasoglu et al. (2019); Danabasoglu (2019a, 2019b, 2019c, 2019d, 2019e)
CESM2-WACCM	NCAR	Danabasoglu et al. (2020)	Danabasoglu (2019f, 2019g, 2019h, 2019i, 2019j, 2019k)
CNRM-CM6-1	CNRM-CERFACS	Voldoire et al. (2019)	Voldoire (2018a, 2018b, 2019e, 2019f, 2019g, 2019h)
CNRM-CM6-1-HR	CNRM-CERFACS	Voldoire et al. (2019)	Voldoire (2019a, 2019b, 2019c, 2019d)
CNRM-ESM2	CNRM-CERFACS	Séférian et al. (2019)	Séférian (2018a, 2018b); Voldoire (2019i, 2019j, 2019k, 2019l)
E3SM-1-0	E3SM Project	Golaz et al. (2019)	Bader et al. (2019a, 2019b)
E3SM-1-1	E3SM Project	Golaz et al. (2019)	Bader et al. (2019c)
EC-Earth3	EC-Earth Consortium	Hazeleger et al. (2012)[a]	EC-Earth Consortium (2019a, 2019b, 2019c)
EC-Earth3-Veg	EC-Earth Consortium	Hazeleger et al. (2012)[a]	EC-Earth Consortium (2019d, 2019e)
FGOALS-f3-L	CAS	He et al. (2019)	Yu (2019a, 2019b, 2019c, 2019d, 2019e, 2019f)
GISS-E2-1-G	NASA-GISS	Schmidt et al. (2014)[a]	NASA-GISS (2018a, 2018b)
GISS-E2-1-G-CC	NASA-GISS	Schmidt et al. (2014)[a]	NASA-GISS (2019)
HadGEM3-GC31-LL	MOHC	Kuhlbrodt et al. (2018)	Ridley et al. (2019a, 2019b); Good (2019, 2020a, 2020b)
HadGEM3-GC31-MM	MOHC	Williams et al. (2018)	Ridley et al. (2019c)
INM-CM4-8	INM	Volodin et al. (2018)	E. Volodin et al. (2019a, 2019b, 2019c, 2019d, 2019e, 2019f)
INM-CM5-0	INM	Volodin et al. (2017)	E. Volodin et al. (2019g, 2019h, 2019i, 2019j, 2019k, 2019l)
IPSL-CM6A-LR	IPSL	Dufresne et al. (2013)[a]	Boucher et al. (2018a, 2018b, 2019a, 2019b, 2019c, 2019d)
MPI-ESM1-2-LR	MPI	Mauritsen et al. (2019)	Wieners et al. (2019a, 2019b, 2019c, 2019d, 2019e)
MPI-ESM1-2-HR	MPI	Müller et al. (2018)	Jungclaus et al. (2019a, 2019b); Schupfner et al. (2019a, 2019b, 2019c, 2019d)
MRI-ESM2-0	MRI	Yukimoto et al. (2019)	Yukimoto, Koshiro, et al. (2019a, 2019b)
NorCPM1	NCC	Counillon et al. (2016)	Bethke et al. (2019)
NorESM2-LM	NCC	Bentsen et al. (2013)[a]	Seland et al. (2019); Seland et al. (2019a, 2019b, 2019c, 2019d)
SAM0-UNICON	SNU	Park et al. (2019)	Park and Shin (2019a, 2019b)
UKESM1-0-LL	MOHC	Sellar et al. (2019)	Tang et al. (2019a, 2019b), Good et al. (2019a, 2019b, 2019c, 2019d)

[a] *To our knowledge*, description papers for several newer model versions have not been published yet, and the reference points to a paper documenting a previous version. Note that NorCPM1 uses data assimilation.

where n is the number of samples and σ is the standard deviation of the sample. There is roughly a 68% (95%) probability that the true mean falls within the range $\mu \pm \sigma_\mu$ ($\mu \pm 2\sigma_\mu$).

2.2. Observational Data

As mentioned in section 1, the RAPID/MOCHA array has been monitoring the AMOC at 26°N since April 2004 (Smeed et al., 2019). We downloaded the data (through September 2018) from www.rapid.ac.uk/rapidmoc and calculated monthly and annual averages from the twice-daily data. The mean AMOC strength (and standard error) at this latitude is 17.7 ± 0.3 Sv for the entire period and 17.4 ± 0.4 Sv for the RAPID period (2005–2014).

The AMOC at 34°S in the South Atlantic has been measured by the South Atlantic MOC Basin-wide Array (SAMBA) project, from March 2009 to April 2017, but with a hiatus from December 2010 to September 2013 (Meinen et al., 2013, 2018). Meinen et al. (2018) and Frajka-Williams et al. (2019) estimate a mean of 14.6 ± 0.7 Sv, but note that the mean is considered the least reliable component of the SAMBA results, as model estimates are used to supplement the observations; see section S3 for a brief discussion. Other estimates based on XBT and Argo float data are about 18 Sv (Dong et al., 2009; Garzoli et al., 2013), while Dong et al. (2015) cite 19.45 Sv based on altimeter data.

Comparison of model-simulated overturning stream function with OSNAP observations is not attempted here. OSNAP reports its overturning estimates in density coordinates (Lozier et al., 2019), and only a few models provided their stream function as such. In addition, OSNAP measures the overturning circulation in two sections that are far from zonal, and it is not straightforward to compare these observations with zonally integrated transports reported by the models.

3. Results

3.1. Validating the Historical AMOC

First, we assess the representation of the AMOC in the CMIP6 models for the historical period. All 27 models simulate a well-defined overturning circulation, associated with North Atlantic Deep Water (NADW) formation in the subpolar North Atlantic Ocean (Figures 1 and S1). At 26°N, several models capture the observed depth of the AMOC maximum (z_{max}) at 1.03 km quite well (Figure 1a), but most have a shallow bias that puts the ensemble-mean depth of the AMOC maximum at 0.84 ± 0.03 km (Table S3). A shallow bias is seen at 34° as well, when compared to estimates from the SAMBA array (Figure 1b). In most models, the depth of the NADW cell at 26°N (defined as the depth z_0 of the zero crossing of the overturning stream function) is between 2.5 and 3.5 km, and the ensemble mean of 3.12 ± 0.14 km is too shallow compared to the RAPID observations (z_0 = 4.40 km). All models display a zero crossing at 34°S, indicating a clear separation between the NADW and AABW cells. Some models display another reversed circulation cell at depth (e.g., INM-CM4-8 at 26°N and HadGEM3-GC31-MM at 34° S).

The ensemble mean overturning strength at 26°N is 17.7 ± 0.8 Sv, within one standard error of the RAPID mean (Table S3), but the spread among models ranges from 9.6 Sv (E3SM-1-1; -1.8σ, where σ is the standard deviation of the ensemble spread) to 23.04 Sv (FGOALS-f3-L; $+1.1\sigma$). The data-assimilated model NorCPM1 is the extreme outlier ($+3.0\sigma$). With an ensemble mean of 16.8 ± 0.7 Sv, CMIP6 models simulate a South Atlantic AMOC that is stronger than the 14.6 Sv that has been inferred from the SAMBA array at 34°S (Meinen et al., 2018) but weaker than some other estimates in the 18-19 Sv range (Dong et al., 2009, 2015; Garzoli et al., 2013). But again, there are significant outliers on both the weak (E3SM; -1.7σ) and strong (NorCPM1; $+2.2\sigma$) side of the mean. The strength of the Antarctic Bottom Water (AABW) cell in the CMIP6 models at 26°N ranges considerably between 0.0 (SAM0-UNICON; -1.1σ) and −8.5 Sv (FGOALS-f3-L; $+4.2\sigma$), but the ensemble mean is only slightly stronger than observations (−1.8 ± 0.3 Sv compared to −1.0 Sv).

3.2. AMOC Trends in Historical Simulations and 21st Century Projections

The time series of AMOC strength at 26°N and 34°S illustrate the long-term variability (Figure S2). Many models—including the ensemble mean—show a gradual increase in AMOC strength over the earlier part of 20th century, followed by a rapid decline starting in the 1980s, a feature that was not seen in the CMIP5 ensemble (Cheng et al., 2013; Weaver et al., 2012). Even though the ensemble mean AMOC trend over the historical period at 26°N is indistinguishable from zero (Figure 2a), there is a clear compensation between positive AMOC trends up to the 1980s (1.3 ± 0.2 Sv) and negative trends in the final decades of the historical

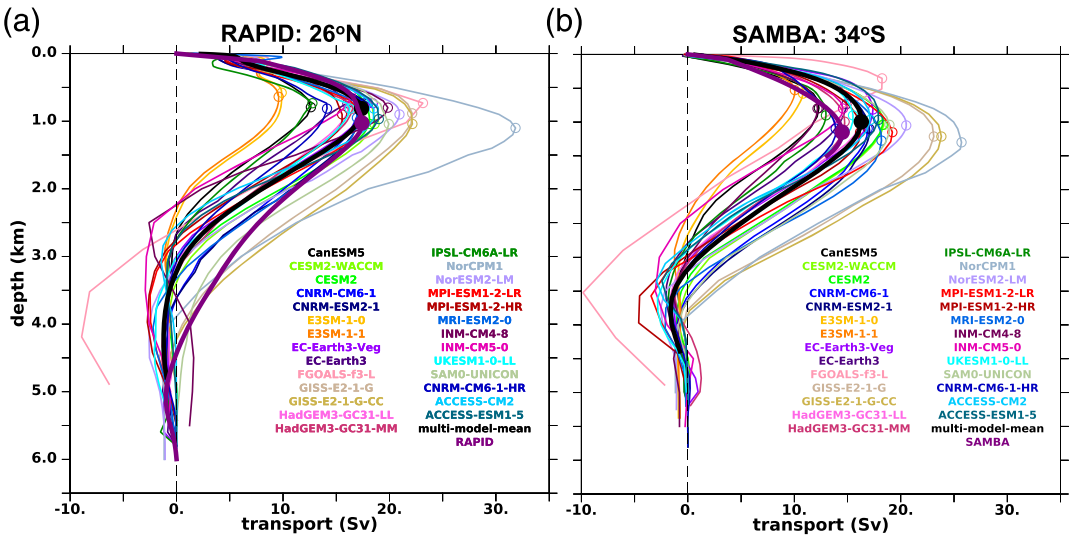

Figure 1. Vertical profiles of the annual mean overturning stream function, evaluated at (a) 26°N and (b) 34°S and averaged over the RAPID period. A single ensemble member from each model is shown, as the ensemble spread is typically small. The location of the maximum stream function value is indicated with a circle. Thick black line and filled circle show the ensemble mean, while thick purple lines and circles show corresponding estimate from the RAPID and SAMBA arrays. Note that the overturning profile of the SAMBA array is estimated for depths shallower than 1,350 dbar only (Meinen et al., 2018).

period (−1.2±0.2 Sv; Figure S3). In fact, only four out of 26 models show a weakening trend between 1850 and 1980. Figure S4 shows that this behavior reflects a compensation between AMOC response to a continuing increase in greenhouse gasses, and to a late-20th century peak in sulfate aerosol forcing (Delworth & Dixon, 2006; Menary et al., 2013).

The 17 models that submitted at least two of the four tier-1 ScenarioMIP simulations all show a decline in AMOC strength over the 21st century (Figure 3). Surprisingly, all models show a rate of decline that is independent of the scenario at least through 2060, while even after 2060 only a few models show an appreciable divergence of the trajectories. This behavior is despite the significant differences among the SSPs in emission scenarios for the radiatively active species (Gidden et al., 2019) and will need more careful evaluation. We note that it is consistent with the emerging notion that many climate variables are proportional to the *cumulative* carbon emissions (Herrington & Zickfeld, 2014; Notz & Stroeve, 2016; Steinacher & Joos, 2016), implying that the AMOC in the first decades of the SSP scenarios is mostly determined by historical CO_2 emissions. Only after the cumulative CO_2 contributions of the SSP scenarios start to become significantly different can the models be expected to diverge. Whether they diverge or not depends on the relative sensitivity of AMOC to CO_2 and the other forcing agents.

Previous model intercomparison studies found that AMOC decline under CO_2 forcing scenarios is stronger in models that have a stronger mean state (e.g., Gregory et al., 2005; Gregory & Tailleux, 2011; Levermann et al., 2007; Weaver et al., 2012; Winton et al., 2014). Indeed, there is weak but statistically significant tendency for models with a weak (strong) mean AMOC to display a positive (negative) trend over the historical period (Figure 2a). However, at face value, this relationship does not seem to be reproduced by the full complement of CMIP6 models considered for SSP simulations (Figures 2c–2f). A closer examination of these plots reveals the presence of outliers. Indeed, a majority of models display a statistically significant linear relationship between projected 21st century AMOC decline and the AMOC mean strength, and similar behavior is also seen in an analysis of AMOC trends in abrupt 4xCO_2 experiments (Figure 2b). A formal cluster analysis presented in section S5 confirms both the existence of outliers and the statistical significance of the linear relationships.

3.3. AMOC and Effective Climate Sensitivity

Recent studies show that the effective climate sensitivity (ECS) of CMIP6 models (defined as the amount of warming resulting from a doubling of the atmospheric CO_2 concentration) is higher than in CMIP5 (Zelinka et al., 2020). Here we document how different AMOC metrics are related to ECS, as determined by

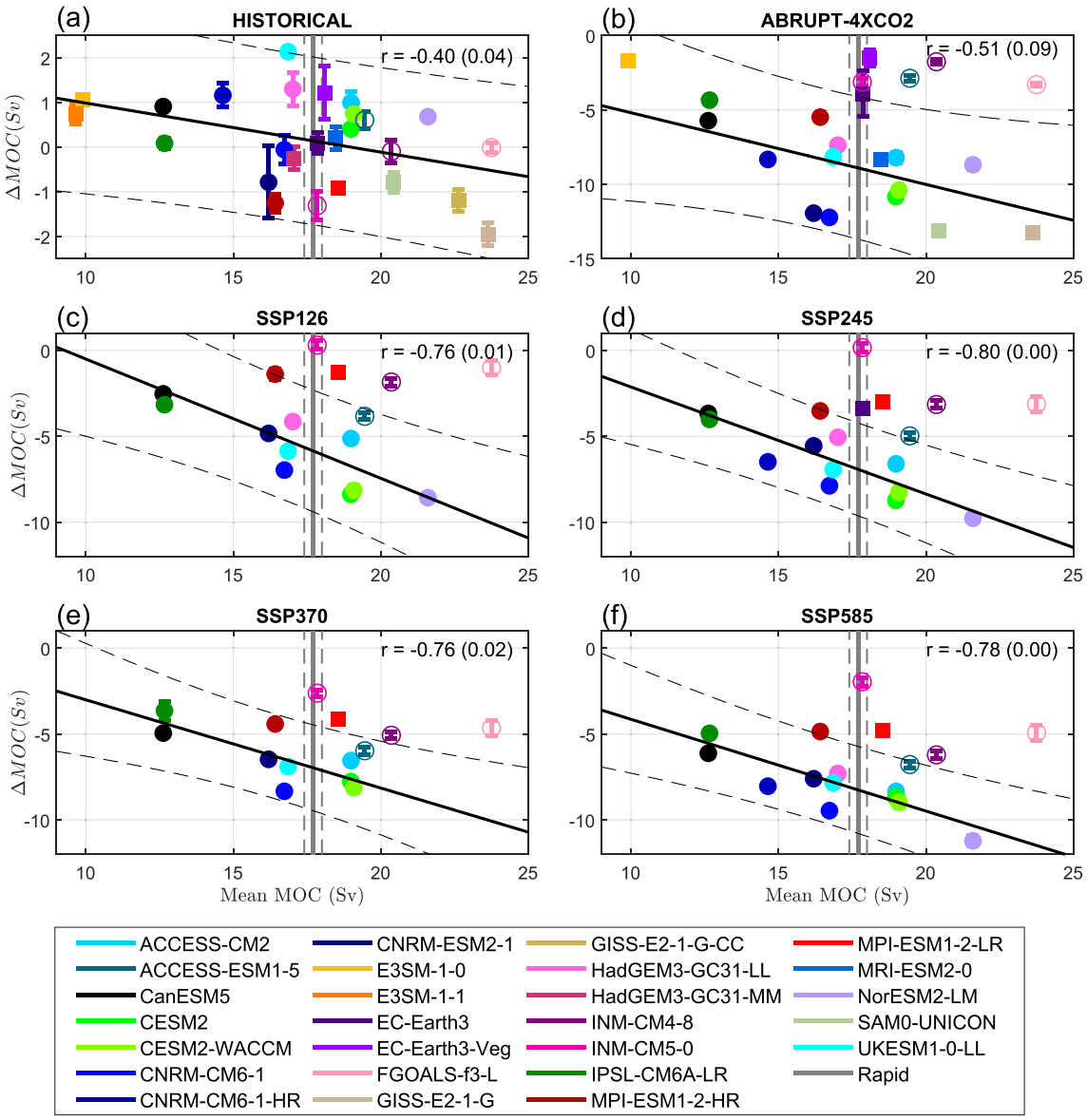

Figure 2. Relationships between AMOC strength at 26°N averaged over the RAPID period, and AMOC changes for (a) historical (RAPID minus 1850–1859); (b) 4xCO_2 (final (141–150) minus first (1–10) decade; and (c–f) the SSP simulations (2091–2100 minus RAPID). Correlation and *p* value are shown in brackets. Solid circles indicate models that belong to the majority cluster, while open circles indicate the cluster of outliers. Models that had not provided abrupt4xCO2, ssp245, and ssp585 simulations by the time of our data freeze were not assigned to a cluster and are indicated by squares. Error bars indicate the standard error over the ensemble. Best linear fit (black solid line; dashed lines showing 95% prediction interval) in (a) is shown for the full ensemble, but in (b–f) for the majority cluster (solid circles) only.

Zelinka et al. (2020) using the method of Gregory et al. (2004) (Table S3). Figure 4a shows a significant inverse relationship between ECS and mean AMOC strength, as models with lower (higher) ECS tend to have stronger (weaker) AMOC mean strength. As could be expected from the linear relationships between mean AMOC and historical AMOC change on the one hand (Figure 2a), and between mean AMOC and ECS on the other hand (Figure 4a), the historical AMOC trends are also proportional to ECS (Figure 4c), with models with low ECS generally displaying negative trends (CO_2 dominated), while models with high ECS tend to display positive trends (aerosol dominated). We expected a similar relationship between ECS and AMOC decline for the 4xCO_2 and SSP experiments, but no such relationship is apparent (Figures 4b and 4d), even if we limit ourselves to the majority cluster.

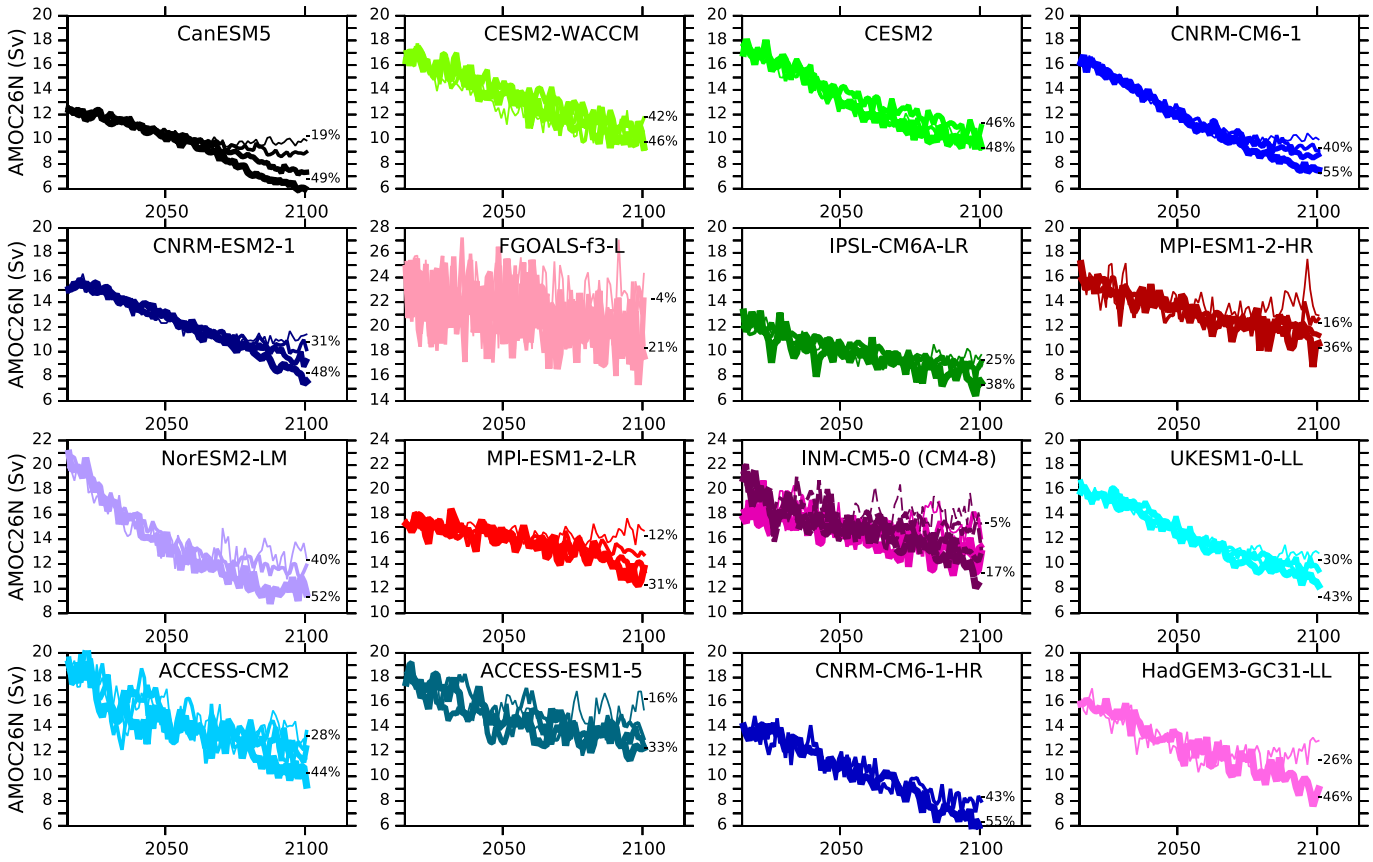

Figure 3. Time series of AMOC at 26°N for the 17 models that submitted AMOC stream function for at least two of the four tier-1 ScenarioMIP simulations (this excludes EC-Earth3). Shown are ensemble means, with progressively thicker lines for the scenarios SSP1-2.6, SSP2-4.5, SSP3-7.0, and SSP5-8.5. Percent decline indicated for the SSP1-2.6 and SSP5-8.5 scenarios compares the 2081–2100 average to historical (1850–2014) mean, per Cheng et al. (2013). In the INM panel, INM-CM4-8 is the darker violet.

4. Discussion and Conclusions

We compare the representation of the AMOC in historical simulations from the CMIP6 multimodel archive to observations from the North (RAPID) and South (SAMBA) Atlantic and study projected AMOC changes in scenario simulations. Our analysis shows that the ensemble mean AMOC strength at 26°N of 27 CMIP6 models agrees within error with RAPID observations, while the AMOC in the South Atlantic is biased strong compared to SAMBA (by 2 Sv). However, model biases persist, including a multimodel-mean NADW cell that is too shallow. Besides, there is still a significant spread in the representation of the AMOC among the models.

The CMIP6 ensemble does not show a significant AMOC trend over the historical period from 1850 to 2014, but many models (and the ensemble mean) display a local maximum in the later part of the 2th century. This behavior reflects a combined effect of the accelerating increase in CO_2 concentrations, and a sulfate aerosol load that peaks in the 1980s, before declining in the 1990s and 2000s (Delworth & Dixon, 2006; Menary et al., 2013). This is at odds with CMIP5 models (Cheng et al., 2013; Weaver et al., 2012), which generally show a weak decline over the 20th century, and with reconstructions based on proxies (Caesar et al., 2018; Rahmstorf et al., 2015; Thornalley et al., 2018).

All models show a decline in the AMOC in the 21st century, with a rate of decline that is independent of emission scenario at least through 2060; only a few models show appreciable divergence between the SSPs thereafter. On average, AMOC decline is 24%, 29%, 32%, and 39% for SSP1-2.6, SSP2-4.5, SSP3-7.0, and SSP5-8.5, respectively. Cheng et al. (2013) and Schleussner et al. (2014) found that CMIP5 models on average displayed a 9% decline for the RCP2.6 scenario (comparable to SSP1-2.6); 21% for RCP4.5 (SSP2-4.5); and

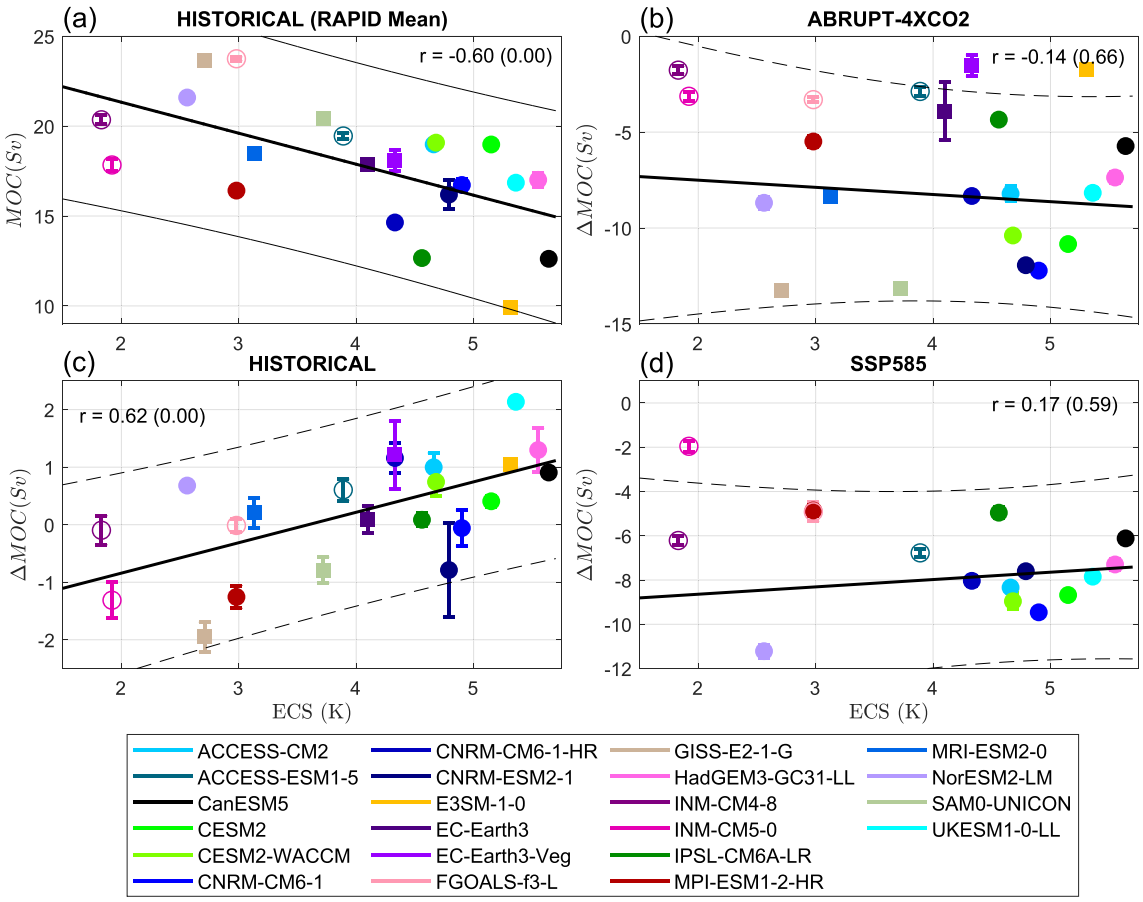

Figure 4. Relationship between ECS and (a) mean AMOC for the RAPID period and AMOC changes for (b) abrupt4xCO2, (c) historical, and (d) ssp585. As in Figure 2, linear trends have been estimated for the full ensemble in panels (a) and (c), while for panels (b) and (d) only the majority cluster (solid circles) were included.

36% for RCP8.5 (SSP5-8.5). The CMIP6 model generation hence projects a stronger decline than CMIP5, with the discrepancy being most pronounced for the scenarios with weakest radiative forcing.

We show that there are two groups of contrasting model behavior, with the majority of models (75% of the 16 models that provided both ssp585 and abrupt4xCO2 simulations), displaying a strong and significant linear relationship between mean present-day AMOC strength and projected 21st century AMOC decline. We can use this "emergent constraint" relationship to calibrate this subensemble with observed mean AMOC state from the RAPID/MOCHA array. For this group, even the low-end scenario (SSP1-2.6, aggressive mitigation) is projected to have a 6 Sv (34%) weaker AMOC by the end of this century (with a range of 2.5 to 9 Sv based on the 95% prediction interval of the linear fit), while the high-end SSP5-8.5 scenario projects a 8 Sv (45%) decline (with a range of 6 to 11 Sv). However, the smaller group of models projects a more moderate AMOC decline of at most 5 Sv (28%) by the end of the 21st century.

Our results support the emerging body of literature that suggests relationships between AMOC mean strength and the role of the AMOC in the climate response to radiative forcing (e.g., Garuba et al., 2018; Rugenstein et al., 2013; Trossman et al., 2016; Winton et al., 2013, 2014). Levermann et al. (2007) argue that the positive relationship between mean AMOC and AMOC decline under CO_2 forcing (Figure 2) is mediated by sea ice. In their view, models with weaker AMOC have generally more Arctic sea ice than models with a stronger AMOC, as a result of the weaker northward heat transport. As the atmosphere warms under enhanced radiative forcing, models with weaker AMOC experience the strongest sea ice retreat, exposing more ocean to the atmosphere. The resulting ocean heat loss counteracts the AMOC weakening induced by atmospheric warming. At the same time, the models with stronger AMOC decline experience stronger reduction in northward heat transport, cooling the subpolar North Atlantic, with implications for sea ice and cloud feedbacks (Garuba et al., 2018; Rugenstein et al., 2013; Trossman et al., 2016; Winton et al., 2013).

This provides a negative feedback on Arctic warming and lowers ECS, consistent with Figures 4a and 4c. It is not obvious why the AMOC decline in 4xCO_2 and SSP simulations does not conform to this picture. However, we speculate that the framework describing the subtle interplay between AMOC and high-latitude feedbacks is no longer valid when large-amplitude forcing perturbations are applied and sea ice is no longer a dominant element in the subpolar North Atlantic and Nordic Seas.

Most models investigated in this study have a nominal ocean resolution of 1°. It is well known that several aspects of the formation (e.g., Pickart et al., 2005), downwelling (e.g., Katsman et al., 2018), and upwelling (e.g., Tamsitt et al., 2017) of deep waters depend on small-scale processes that cannot be explicitly represented by these models. Whether this has biased our estimate of the sensitivity of the AMOC to climate forcing is an important question that will need to be addressed using century-long scenario experiments with high-resolution models. Here we note that the few models that submitted simulations at higher resolutions (CNRM-CM6, MPI-ESM1-2, and HadGEM3-GC31) do not stand out from the rest of the ensemble, consistent with the conclusion from Winton et al. (2014) that spatial resolution in itself does not impact AMOC sensitivity to radiative forcing.

Acknowledgments
We acknowledge the World Climate Research Programme, which, through its Working Group on Coupled Modelling, coordinated and promoted CMIP6. We thank the Earth System Grid Federation (ESGF) for archiving the data and providing access; the multiple funding agencies who support CMIP6 and ESGF; DOE's RGMA program area, the Data Management program, and NERSC for making this coordinated CMIP6 analysis activity possible; and the modeling centers for generously sharing their CMIP6 model output. CMIP6 model data are licensed under a Creative Commons Attribution-ShareAlike 4.0 International License (https://creativecommons.org/licenses) and can be accessed through the ESGF nodes (for instance esgf-node.llnl.gov/search/cmip6). We like to thank three anonymous reviewers for their constructive comments and Jian Lu (PNNL) and Christopher Meinen (NOAA/AOML) for useful discussions. Data from the RAPID/MOCHA program and the RAPID-WATCH MOC monitoring project are funded by the Natural Environment Research Council and the U.S. National Science Foundation and are freely available online from (www.rapid.ac.uk/rapidmoc). Data from the Southwest Atlantic MOC project (SAM) are funded by the DOC-NOAA Climate Program Office-Ocean Observation and Monitoring Division and the Atlantic Oceanographic and Meteorological Laboratory. These data are freely available online (via www.aoml.noaa.gov/phod/research/moc/samoc/sam). This research was supported by the Regional and Global Model Analysis (RGMA) component of the Earth and Environmental System Modeling (EESM) program of the U.S. Department of Energy's Office of Science, as contribution to the HiLAT-RASM and CATALYST projects, and by the National Science Foundation IA 1947282. Cheng is supported by NOAA CPO CVP Program under Grant NA16OAR4310169. This publication is partially funded by the Joint Institute for the Study of the Atmosphere and Ocean (JISAO) under NOAA Cooperative Agreement NA15OAR4320063, Contribution No. 2019-1035. This is PMEL Contribution 5032.

References

Bader, D. C., Leung, R., Taylor, M., & McCoy, R. B. (2019a). E3SM-Project E3SM1.0 model output prepared for CMIP6 CMIP abrupt-4xCO2. Earth System Grid Federation. https://doi.org/10.22033/ESGF/CMIP6.4491

Bader, D. C., Leung, R., Taylor, M., & McCoy, R. B. (2019b). E3SM-Project E3SM1.0 model output prepared for CMIP6 CMIP historical. Earth System Grid Federation. https://doi.org/10.22033/ESGF/CMIP6.4497

Bader, D. C., Leung, R., Taylor, M., & McCoy, R. B. (2019c). E3SM-Project E3SM1.1 model output prepared for CMIP6 CMIP historical. Earth System Grid Federation. http://doi.org/10.22033/ESGF/CMIP6.11485

Bentsen, M., Bethke, I., Debernard, J., Iversen, T., Kirkevåg, A., Seland, Ø., et al. (2013). The Norwegian Earth system model, NorESM1-M-Part 1: Description and basic evaluation of the physical climate. *Geoscientific Model Development*, *6*(3), 687–720.

Bethke, I., Wang, Y., Counillon, F., Kimmritz, M., Fransner, F., Samuelsen, A., et al. (2019). NCC NorCPM1 model output prepared for CMIP6 CMIP historical. Earth System Grid Federation. https://doi.org/10.22033/ESGF/CMIP6.10894

Bi, D., Dix, M., Marsland, S. J., O'Farrell, S., Rashid, H., Uotila, P., et al. (2013). The ACCESS coupled model: Description, control climate and evaluation. *Australian Meteorological and Oceanographic Journal*, *63*(1), 41–64.

Boucher, O., Denvil, S., Caubel, A., & Foujols, M. A. (2018a). IPSL IPSL-CM6A-LR model output prepared for CMIP6 CMIP abrupt-4xCO2. Earth System Grid Federation. https://doi.org/10.22033/ESGF/CMIP6.5109

Boucher, O., Denvil, S., Caubel, A., & Foujols, M. A. (2018b). IPSL IPSL-CM6A-LR model output prepared for CMIP6 CMIP historical. Earth System Grid Federation. https://doi.org/10.22033/ESGF/CMIP6.5195

Boucher, O., Denvil, S., Caubel, A., & Foujols, M. A. (2019a). IPSL IPSL-CM6A-LR model output prepared for CMIP6 ScenarioMIP ssp126. Earth System Grid Federation. https://doi.org/10.22033/ESGF/CMIP6.5262

Boucher, O., Denvil, S., Caubel, A., & Foujols, M. A. (2019b). IPSL IPSL-CM6A-LR model output prepared for CMIP6 ScenarioMIP ssp245. Earth System Grid Federation. https://doi.org/10.22033/ESGF/CMIP6.5264

Boucher, O., Denvil, S., Caubel, A., & Foujols, M. A. (2019c). IPSL IPSL-CM6A-LR model output prepared for CMIP6 ScenarioMIP ssp370. Earth System Grid Federation. https://doi.org/10.22033/ESGF/CMIP6.5265

Boucher, O., Denvil, S., Caubel, A., & Foujols, M. A. (2019d). IPSL IPSL-CM6A-LR model output prepared for CMIP6 ScenarioMIP ssp585. Earth System Grid Federation. https://doi.org/10.22033/ESGF/CMIP6.5271

Bryden, H. L., Longworth, H. R., & Cunningham, S. A. (2005). Slowing of the Atlantic meridional overturning circulation at 25 N. *Nature*, *438*(7068), 655.

Caesar, L., Rahmstorf, S., Robinson, A., Feulner, G., & Saba, V. (2018). Observed fingerprint of a weakening Atlantic Ocean overturning circulation. *Nature*, *556*(7700), 191.

Carlson, C. A., Hansell, D. A., Nelson, N. B., Siegel, D. A., Smethie, W. M., Khatiwala, S., et al. (2010). Dissolved organic carbon export and subsequent remineralization in the mesopelagic and bathypelagic realms of the North Atlantic basin. *Deep Sea Research Part II: Topical Studies in Oceanography*, *57*(16), 1433–1445.

Cheng, W., Chiang, J. C., & Zhang, D. (2013). Atlantic meridional overturning circulation (AMOC) in CMIP5 models: RCP and historical simulations. *Journal of Climate*, *26*(18), 7187–7197.

Counillon, F., Keenlyside, N., Bethke, I., Wang, Y., Billeau, S., Shen, M. L., & Bentsen, M. (2016). Flow-dependent assimilation of sea surface temperature in isopycnal coordinates with the Norwegian Climate Prediction Model. *Tellus A: Dynamic Meteorology and Oceanography*, *68*(1), 32,437.

Danabasoglu, G. (2019a). NCAR CESM2 model output prepared for CMIP6 CMIP abrupt-4xCO2. Earth System Grid Federation. https://doi.org/10.22033/ESGF/CMIP6.7519

Danabasoglu, G. (2019b). NCAR CESM2 model output prepared for CMIP6 ScenarioMIP ssp126. Earth System Grid Federation. https://doi.org/10.22033/ESGF/CMIP6.7746

Danabasoglu, G. (2019c). NCAR CESM2 model output prepared for CMIP6 ScenarioMIP ssp245. Earth System Grid Federation. https://doi.org/10.22033/ESGF/CMIP6.7748

Danabasoglu, G. (2019d). NCAR CESM2 model output prepared for CMIP6 ScenarioMIP ssp370. Earth System Grid Federation. https://doi.org/10.22033/ESGF/CMIP6.7753

Danabasoglu, G. (2019e). NCAR CESM2 model output prepared for CMIP6 ScenarioMIP ssp585. Earth System Grid Federation. https://doi.org/10.22033/ESGF/CMIP6.7768

Danabasoglu, G. (2019f). NCAR CESM2-WACCM model output prepared for CMIP6 CMIP abrupt-4xCO2. Earth System Grid Federation. https://doi.org/10.22033/ESGF/CMIP6.10039

Danabasoglu, G. (2019g). NCAR CESM2-WACCM model output prepared for CMIP6 CMIP historical. Earth System Grid Federation. https://doi.org/10.22033/ESGF/CMIP6.10071

Danabasoglu, G. (2019h). NCAR CESM2-WACCM model output prepared for CMIP6 ScenarioMIP ssp126. Earth System Grid Federation. https://doi.org/10.22033/ESGF/CMIP6.10100
Danabasoglu, G. (2019i). NCAR CESM2-WACCM model output prepared for CMIP6 ScenarioMIP ssp245. Earth System Grid Federation. https://doi.org/10.22033/ESGF/CMIP6.10101
Danabasoglu, G. (2019j). NCAR CESM2-WACCM model output prepared for CMIP6 ScenarioMIP ssp370. Earth System Grid Federation. https://doi.org/10.22033/ESGF/CMIP6.10102
Danabasoglu, G. (2019k). NCAR CESM2-WACCM model output prepared for CMIP6 ScenarioMIP ssp585. Earth System Grid Federation. https://doi.org/10.22033/ESGF/CMIP6.10115
Danabasoglu, G., Lamarque, J. F., Bachmeister, J., Bailey, D. A., DuVivier, A. K., Edwards, J., et al. (2020). The Community Earth System Model Version 2 (CESM2). *Journal of Advances in Modeling Earth Systems*, *12*, e01916. https://doi.org/10.1029/2019MS001916
Danabasoglu, G., Lawrence, D., Lindsay, K., Lipscomb, W., & Strand, G. (2019). NCAR CESM2 model output prepared for CMIP6 CMIP historical. Earth System Grid Federation. https://doi.org/10.22033/ESGF/CMIP6.7627
Day, J., Hargreaves, J., Annan, J., & Abe-Ouchi, A. (2012). Sources of multi-decadal variability in Arctic sea ice extent. *Environmental Research Letters*, *7*(3), 034011.
Delworth, T. L., & Dixon, K. W. (2006). Have anthropogenic aerosols delayed a greenhouse gas-induced weakening of the North Atlantic thermohaline circulation? *Geophysical Research Letters*, *33*, L02606. https://doi.org/10.1029/2005GL024980
Dix, M., Bi, D., Dobrohotoff, P., Fiedler, R., Harman, I., Law, R., & Yang, R. (2019a). CSIRO-ARCCSS ACCESS-CM2 model output prepared for CMIP6 CMIP abrupt-4xCO2. Earth System Grid Federation. https://doi.org/10.22033/ESGF/CMIP6.4237
Dix, M., Bi, D., Dobrohotoff, P., Fiedler, R., Harman, I., Law, R., & Yang, R. (2019b). CSIRO-ARCCSS ACCESS-CM2 model output prepared for CMIP6 CMIP historical. Earth System Grid Federation. https://doi.org/10.22033/ESGF/CMIP6.4271
Dix, M., Bi, D., Dobrohotoff, P., Fiedler, R., Harman, I., Law, R., & Yang, R. (2019c). CSIRO-ARCCSS ACCESS-CM2 model output prepared for CMIP6 ScenarioMIP ssp126. Earth System Grid Federation. https://doi.org/10.22033/ESGF/CMIP6.4319
Dix, M., Bi, D., Dobrohotoff, P., Fiedler, R., Harman, I., Law, R., & Yang, R. (2019d). CSIRO-ARCCSS ACCESS-CM2 model output prepared for CMIP6 ScenarioMIP ssp245. Earth System Grid Federation. https://doi.org/10.22033/ESGF/CMIP6.4321
Dix, M., Bi, D., Dobrohotoff, P., Fiedler, R., Harman, I., Law, R., & Yang, R. (2019e). CSIRO-ARCCSS ACCESS-CM2 model output prepared for CMIP6 ScenarioMIP ssp370. Earth System Grid Federation. https://doi.org/10.22033/ESGF/CMIP6.4323
Dix, M., Bi, D., Dobrohotoff, P., Fiedler, R., Harman, I., Law, R., & Yang, R. (2019f). CSIRO-ARCCSS ACCESS-CM2 model output prepared for CMIP6 ScenarioMIP ssp585. Earth System Grid Federation. https://doi.org/10.22033/ESGF/CMIP6.4332
Dong, S., Garzoli, S., Baringer, M., Meinen, C., & Goni, G. (2009). Interannual variations in the Atlantic meridional overturning circulation and its relationship with the net northward heat transport in the South Atlantic. *Geophysical Research Letters*, *36*, L20606. https://doi.org/10.1029/2009GL039356
Dong, S., Goni, G., & Bringas, F. (2015). Temporal variability of the South Atlantic meridional overturning circulation between 20°S and 35°S. *Geophysical Research Letters*, *42*, 7655–7662. https://doi.org/10.1002/2015GL065603
Dufresne, J. L., Foujols, M. A., Denvil, S., Caubel, A., Marti, O., Aumont, O., et al. (2013). Climate change projections using the IPSL-CM5 Earth System Model: from CMIP3 to CMIP5. *Climate Dynamics*, *40*(9-10), 2123–2165.
EC-Earth Consortium (2019a). EC-Earth-Consortium EC-Earth3 model output prepared for CMIP6 CMIP abrupt-4xCO2. Earth System Grid Federation. https://doi.org/10.22033/ESGF/CMIP6.4518
EC-Earth Consortium (2019b). EC-Earth-Consortium EC-Earth3 model output prepared for CMIP6 CMIP historical. Earth System Grid Federation. https://doi.org/10.22033/ESGF/CMIP6.4700
EC-Earth Consortium (2019c). EC-Earth-Consortium EC-Earth3 model output prepared for CMIP6 ScenarioMIP ssp245. Earth System Grid Federation. https://doi.org/10.22033/ESGF/CMIP6.4880
EC-Earth Consortium (2019d). EC-Earth-Consortium EC-Earth3-Veg model output prepared for CMIP6 CMIP abrupt-4xCO2. Earth System Grid Federation. https://doi.org/10.22033/ESGF/CMIP6.4524
EC-Earth Consortium (2019e). EC-Earth-Consortium EC-Earth3-Veg model output prepared for CMIP6 CMIP historical. Earth System Grid Federation. https://doi.org/10.22033/ESGF/CMIP6.4706
Eyring, V., Bony, S., Meehl, G. A., Senior, C. A., Stevens, B., Stouffer, R. J., & Taylor, K. E. (2016). Overview of the Coupled Model Intercomparison Project Phase 6 (CMIP6) experimental design and organization. *Geoscientific Model Development*, *9*(LLNL-JRNL-736881), 1937–1958. https://doi.org/10.5194/gmd-9-1937-2016
Fontela, M., García-Ibáñez, M. I., Hansell, D. A., Mercier, H., & Pérez, F. F. (2016). Dissolved organic carbon in the North Atlantic meridional overturning circulation. *Scientific Reports*, *6*, 26,931.
Frajka-Williams, E., Ansorge, I. J., Baehr, J., Bryden, H. L., Chidichimo, M. P., Cunningham, S. A., et al. (2019). Atlantic meridional overturning circulation: Observed transports and variability. *Frontiers in Marine Science*, *6*, 260.
Garuba, O. A., Lu, J., Liu, F., & Singh, H. A. (2018). The active role of the ocean in the temporal evolution of climate sensitivity. *Geophysical Research Letters*, *45*, 306–315. https://doi.org/10.1002/2017GL075633
Garzoli, S. L., Baringer, M. O., Dong, S., Perez, R. C., & Yao, Q. (2013). South Atlantic meridional fluxes. *Deep Sea Research Part I: Oceanographic Research Papers*, *71*, 21–32.
Gidden, M., Riahi, K., Smith, S., Fujimori, S., Luderer, G., Kriegler, E., et al. (2019). Global emissions pathways under different socioeconomic scenarios for use in CMIP6: A dataset of harmonized emissions trajectories through the end of the century. *Geoscientific Model Development*, *12*(4), 1443–1475. https://doi.org/10.5194/gmd-12-1443-2019
Golaz, J. C., Caldwell, P. M., Van Roekel, L. P., Petersen, M. R., Tang, Q., Wolfe, J. D., et al. (2019). The DOE E3SM coupled model Version 1: Overview and evaluation at standard resolution. *Journal of Advances in Modeling Earth Systems*, *11*, 2089–2129.
Good, P. (2019). MOHC HadGEM3-GC31-LL model output prepared for CMIP6 ScenarioMIP ssp245. Earth System Grid Federation. https://doi.org/10.22033/ESGF/CMIP6.10851
Good, P. (2020a). MOHC HadGEM3-GC31-LL model output prepared for CMIP6 ScenarioMIP ssp126. Earth System Grid Federation. https://doi.org/10.22033/ESGF/CMIP6.10849
Good, P. (2020b). MOHC HadGEM3-GC31-LL model output prepared for CMIP6 ScenarioMIP ssp585. Earth System Grid Federation. https://doi.org/10.22033/ESGF/CMIP6.10901
Good, P., Sellar, A., Tang, Y., Rumbold, S., Ellis, R., Kelley, D., & Kuhlbrodt, T. (2019a). MOHC UKESM1.0-LL model output prepared for CMIP6 ScenarioMIP ssp126. Earth System Grid Federation. https://doi.org/10.22033/ESGF/CMIP6.6333
Good, P., Sellar, A., Tang, Y., Rumbold, S., Ellis, R., Kelley, D., & Kuhlbrodt, T. (2019b). MOHC UKESM1.0-LL model output prepared for CMIP6 ScenarioMIP ssp245. Earth System Grid Federation. https://doi.org/10.22033/ESGF/CMIP6.6339
Good, P., Sellar, A., Tang, Y., Rumbold, S., Ellis, R., Kelley, D., & Kuhlbrodt, T. (2019c). MOHC UKESM1.0-LL model output prepared for CMIP6 ScenarioMIP ssp370. Earth System Grid Federation. https://doi.org/10.22033/ESGF/CMIP6.6347

Good, P., Sellar, A., Tang, Y., Rumbold, S., Ellis, R., Kelley, D., & Kuhlbrodt, T. (2019d). MOHC UKESM1.0-LL model output prepared for CMIP6 ScenarioMIP ssp585. Earth System Grid Federation. https://doi.org/10.22033/ESGF/CMIP6.6405

Gregory, J. M., Dixon, K. W., Stouffer, R. J., Weaver, A. J., Driesschaert, E., Eby, M., et al. (2005). A model intercomparison of changes in the Atlantic thermohaline circulation in response to increasing atmospheric CO2 concentration. *Geophysical Research Letters*, *32*, L12703. https://doi.org/10.1029/2005GL023209

Gregory, J. M., Ingram, W. J., Palmer, M. A., Jones, G. S., Stott, P. A., Thorpe, R. B., et al. (2004). A new method for diagnosing radiative forcing and climate sensitivity. *Geophysical Research Letters*, *31*, L03205. https://doi.org/10.1029/2003GL018747

Gregory, J. M., & Tailleux, R. (2011). Kinetic energy analysis of the response of the Atlantic meridional overturning circulation to CO_2-forced climate change. *Climate Dynamics*, *37*(5-6), 893–914.

Häkkinen, S., Rhines, P. B., & Worthen, D. L. (2015). Heat content variability in the North Atlantic Ocean in ocean reanalyses. *Geophysical Research Letters*, *42*, 2901–2909. https://doi.org/10.1002/2015GL063299

Hall, A., Cox, P., Huntingford, C., & Klein, S. (2019). Progressing emergent constraints on future climate change. *Nature Climate Change*, *9*(4), 269–278.

Hazeleger, W., Wang, X., Severijns, C., Ştefănescu, S., Bintanja, R., Sterl, A., et al. (2012). EC-Earth V2. 2: Description and validation of a new seamless earth system prediction model. *Climate Dynamics*, *39*(11), 2611–2629.

He, B., Bao, Q., Wang, X., Zhou, L., Wu, X., Liu, Y., et al. (2019). CAS FGOALS-f3-L model datasets for CMIP6 historical atmospheric model intercomparison project simulation. *Advances in Atmospheric Sciences*, *36*(8), 771–778.

Herrington, T., & Zickfeld, K. (2014). Path independence of climate and carbon cycle response over a broad range of cumulative carbon emissions. *Earth System Dynamics*, *5*(2), 409.

Hoesly, R. M., Smith, S. J., Feng, L., Klimont, Z., Janssens-Maenhout, G., Pitkanen, T., et al. (2018). Historical (1750–2014) anthropogenic emissions of reactive gases and aerosols from the Community Emissions Data System (CEDS). *Geoscientific Model Development*, *11*(PNNL-SA-123932), 369–408. https://doi.org/10.5194/gmd-11-369-2018

Johns, W. E., Baringer, M. O., Beal, L. M., Cunningham, S., Kanzow, T., Bryden, H. L., et al. (2011). Continuous, array-based estimates of Atlantic Ocean heat transport at 26.5°N. *Journal of Climate*, *24*(10), 2429–2449.

Jungclaus, J., Bittner, M., Wieners, K. H., Wachsmann, F., Schupfner, M., Legutke, S., et al. (2019a). MPI-M MPI-ESM1.2-HR model output prepared for CMIP6 CMIP abrupt-4xCO2. Earth System Grid Federation. https://doi.org/10.22033/ESGF/CMIP6.6458

Jungclaus, J., Bittner, M., Wieners, K. H., Wachsmann, F., Schupfner, M., Legutke, S., et al. (2019b). MPI-M MPI-ESM1.2-HR model output prepared for CMIP6 CMIP historical. Earth System Grid Federation. https://doi.org/10.22033/ESGF/CMIP6.6594

Katsman, C. A., Drijfhout, S., Dijkstra, H. A., & Spall, M. A. (2018). Sinking of dense North Atlantic waters in a global ocean model: Location and controls. *Journal of Geophysical Research: Oceans*, *123*, 3563–3576. https://doi.org/10.1029/2017JC013329

Kostov, Y., Armour, K. C., & Marshall, J. (2014). Impact of the Atlantic meridional overturning circulation on ocean heat storage and transient climate change. *Geophysical Research Letters*, *41*, 2108–2116. https://doi.org/10.1002/2013GL058998

Kuhlbrodt, T., Jones, C. G., Sellar, A., Storkey, D., Blockley, E., Stringer, M., et al. (2018). The low-resolution version of HadGEM3 GC3. 1: Development and evaluation for global climate. *Journal of Advances in Modeling Earth Systems*, *10*, 2865–2888. https://doi.org/10.1029/2018MS001370

Law, R. M., Ziehn, T., Matear, R. J., Lenton, A., Chamberlain, M. A., Stevens, L. E., et al. (2017). The carbon cycle in the Australian Community Climate and Earth System Simulator (ACCESS-ESM1)–Part 1: Model description and pre-industrial simulation. *Geoscientific Model Development*, *10*(7), 2567.

Levermann, A., Mignot, J., Nawrath, S., & Rahmstorf, S. (2007). The role of northern sea ice cover for the weakening of the thermohaline circulation under global warming. *Journal of Climate*, *20*(16), 4160–4171.

Lozier, M., Li, F., Bacon, S., Bahr, F., Bower, A., Cunningham, S., et al. (2019). A sea change in our view of overturning in the subpolar North Atlantic. *Science*, *363*(6426), 516–521.

Mahajan, S., Zhang, R., & Delworth, T. L. (2011). Impact of the Atlantic meridional overturning circulation (AMOC) on Arctic surface air temperature and sea ice variability. *Journal of Climate*, *24*(24), 6573–6581.

Marshall, J., Donohoe, A., Ferreira, D., & McGee, D. (2014). The ocean's role in setting the mean position of the Inter-Tropical Convergence Zone. *Climate Dynamics*, *42*(7-8), 1967–1979.

Mauritsen, T., Bader, J., Becker, T., Behrens, J., Bittner, M., Brokopf, R., et al. (2019). Developments in the MPI-M Earth System Model Version 1.2 (MPI-ESM1. 2) and its response to increasing CO2. *Journal of Advances in Modeling Earth Systems*, *11*, 998–1038. https://doi.org/10.1029/2018MS001400

Meinen, C. S., Speich, S., Perez, R. C., Dong, S., Piola, A. R., Garzoli, S. L., et al. (2013). Temporal variability of the meridional overturning circulation at 34.5°S: Results from two pilot boundary arrays in the South Atlantic. *Journal of Geophysical Research: Oceans*, *118*, 6461–6478. https://doi.org/10.1002/2013JC009228

Meinen, C. S., Speich, S., Piola, A. R., Ansorge, I., Campos, E., Kersalé, M., et al. (2018). Meridional overturning circulation transport variability at 34.5°S during 2009–2017: Baroclinic and barotropic flows and the dueling influence of the boundaries. *Geophysical Research Letters*, *45*, 4180–4188. https://doi.org/10.1029/2018GL077408

Meinshausen, M., Vogel, E., Nauels, A., Lorbacher, K., Meinshausen, N., Etheridge, D. M., et al. (2017). Historical greenhouse gas concentrations for climate modelling (CMIP6). *Geoscientific Model Development*, *10*, 2057–2116.

Menary, M. B., Roberts, C. D., Palmer, M. D., Halloran, P. R., Jackson, L., Wood, R. A., et al. (2013). Mechanisms of aerosol-forced AMOC variability in a state of the art climate model. *Journal of Geophysical Research: Oceans*, *118*, 2087–2096. https://doi.org/10.1002/jgrc.20178

Müller, W. A., Jungclaus, J. H., Mauritsen, T., Baehr, J., Bittner, M., Budich, R., et al. (2018). A higher-resolution version of the Max Planck Institute Earth System Model (MPI-ESM1. 2-HR). *Journal of Advances in Modeling Earth Systems*, *10*, 1383–1413. https://doi.org/10.1029/2017MS001217

NASA-GISS (2018a). NASA-GISS GISS-E2.1G model output prepared for CMIP6 CMIP abrupt-4xCO2. Earth System Grid Federation. https://doi.org/10.22033/ESGF/CMIP6.6976

NASA-GISS (2018b). NASA-GISS GISS-E2.1G model output prepared for CMIP6 CMIP historical. Earth System Grid Federation. https://doi.org/10.22033/ESGF/CMIP6.7127

NASA-GISS (2019). NASA-GISS GISS-E2-1-G-CC model output prepared for CMIP6 CMIP historical. Earth System Grid Federation. https://doi.org/10.22033/ESGF/CMIP6.11762

Notz, D., & Stroeve, J. (2016). Observed Arctic sea-ice loss directly follows anthropogenic CO2 emission. *Science*, *354*(6313), 747–750.

O'Neill, B. C., Tebaldi, C., Vuuren, D. P. V., Eyring, V., Friedlingstein, P., Hurtt, G., et al. (2016). The scenario model intercomparison project (ScenarioMIP) for CMIP6. *Geoscientific Model Development*, *9*(9), 3461–3482. https://doi.org/10.5194/gmd-9-3461-2016

Palter, J. B. (2015). The role of the Gulf Stream in European climate. *Annual Review of Marine Science*, *7*, 113–137.

Park, S., & Shin, J. (2019a). SNU SAM0-UNICON model output prepared for CMIP6 CMIP abrupt-4xCO2. Earth System Grid Federation. https://doi.org/10.22033/ESGF/CMIP6.7783
Park, S., & Shin, J. (2019b). SNU SAM0-UNICON model output prepared for CMIP6 CMIP historical. Earth System Grid Federation. https://doi.org/10.22033/ESGF/CMIP6.7789
Park, S., Shin, J., Kim, S., Oh, E., & Kim, Y. (2019). Global climate simulated by the Seoul National University Atmosphere Model Version 0 with a Unified Convection Scheme (SAM0-UNICON). *Journal of Climate*, *32*(10), 2917–2949.
Pickart, R. S., Torres, D. J., & Fratantoni, P. S. (2005). The east Greenland spill jet. *Journal of Physical Oceanography*, *35*(6), 1037–1053.
Rahmstorf, S., Box, J. E., Feulner, G., Mann, M. E., Robinson, A., Rutherford, S., & Schaffernicht, E. J. (2015). Exceptional twentieth-century slowdown in Atlantic Ocean overturning circulation. *Nature Climate Change*, *5*(5), 475.
Ridley, J., Menary, M., Kuhlbrodt, T., Andrews, M., & Andrews, T. (2019a). MOHC HadGEM3-GC31-LL model output prepared for CMIP6 CMIP abrupt-4xCO2. Earth System Grid Federation. https://doi.org/10.22033/ESGF/CMIP6.5839
Ridley, J., Menary, M., Kuhlbrodt, T., Andrews, M., & Andrews, T. (2019b). MOHC HadGEM3-GC31-LL model output prepared for CMIP6 CMIP historical. Earth System Grid Federation. https://doi.org/10.22033/ESGF/CMIP6.6109
Ridley, J., Menary, M., Kuhlbrodt, T., Andrews, M., & Andrews, T. (2019c). MOHC HadGEM3-GC31-MM model output prepared for CMIP6 CMIP historical. Earth System Grid Federation. https://doi.org/10.22033/ESGF/CMIP6.6112
Rugenstein, M. A., Winton, M., Stouffer, R. J., Griffies, S. M., & Hallberg, R. (2013). Northern high-latitude heat budget decomposition and transient warming. *Journal of climate*, *26*(2), 609–621.
Schleussner, C. F., Levermann, A., & Meinshausen, M. (2014). Probabilistic projections of the Atlantic overturning. *Climatic change*, *127*(3-4), 579–586.
Schmidt, G. A., Kelley, M., Nazarenko, L., Ruedy, R., Russell, G. L., Aleinov, I., et al. (2014). Configuration and assessment of the GISS ModelE2 contributions to the CMIP5 archive. *Journal of Advances in Modeling Earth Systems*, *6*, 141–184. https://doi.org/10.1002/2013MS000265
Schupfner, M., Wieners, K. H., Wachsmann, F., Steger, C., Bittner, M., Jungclaus, J., & Roeckner, E. (2019a). DKRZ MPI-ESM1.2-HR model output prepared for CMIP6 ScenarioMIP ssp126. Earth System Grid Federation. https://doi.org/10.22033/ESGF/CMIP6.4397
Schupfner, M., Wieners, K. H., Wachsmann, F., Steger, C., Bittner, M., Jungclaus, J., & Roeckner, E. (2019b). DKRZ MPI-ESM1.2-HR model output prepared for CMIP6 ScenarioMIP ssp245. Earth System Grid Federation. https://doi.org/10.22033/ESGF/CMIP6.4398
Schupfner, M., Wieners, K. H., Wachsmann, F., Steger, C., Bittner, M., Jungclaus, J., & Roeckner, E. (2019c). DKRZ MPI-ESM1.2-HR model output prepared for CMIP6 ScenarioMIP ssp370. Earth System Grid Federation. https://doi.org/10.22033/ESGF/CMIP6.4399
Schupfner, M., Wieners, K. H., Wachsmann, F., Steger, C., Bittner, M., Jungclaus, J., & Roeckner, E. (2019d). DKRZ MPI-ESM1.2-HR model output prepared for CMIP6 ScenarioMIP ssp585. Earth System Grid Federation. https://doi.org/10.22033/ESGF/CMIP6.4403
Séférian, R. (2018a). CNRM-CERFACS CNRM-ESM2-1 model output prepared for CMIP6 CMIP for experiment abrupt-4xCO2. Earth System Grid Federation. https://doi.org/10.22033/ESGF/CMIP6.3918
Séférian, R. (2018b). CNRM-CERFACS CNRM-ESM2-1 model output prepared for CMIP6 CMIP historical. Earth System Grid Federation. https://doi.org/10.22033/ESGF/CMIP6.4068
Séférian, R., Nabat, P., Michou, M., Saint-Martin, D., Voldoire, A., Colin, J., et al. (2019). Evaluation of CNRM Earth-System model, CNRM-ESM2-1: role of Earth system processes in present-day and future climate. *Journal of Advances in Modeling Earth Systems*, *11*, 4182–4227. https://doi.org/10.1029/2019MS001791
Seland, Y., Bentsen, M., Oliviè, D. J. L., Toniazzo, T., Gjermundsen, A., Graff, L. S., & Schulz, M. (2019). NCC NorESM2-LM model output prepared for CMIP6 CMIP abrupt-4xCO2. Earth System Grid Federation. https://doi.org/10.22033/ESGF/CMIP6.7836
Seland, Ø., Bentsen, M., Oliviè, D. J. L., Toniazzo, T., Gjermundsen, A., Graff, L. S., et al. (2019a). NCC NorESM2-LM model output prepared for CMIP6 CMIP historical. Earth System Grid Federation. https://doi.org/10.22033/ESGF/CMIP6.8036
Seland, Ø., Bentsen, M., Oliviè, D. J. L., Toniazzo, T., Gjermundsen, A., Graff, L. S., et al. (2019b). NCC NorESM2-LM model output prepared for CMIP6 ScenarioMIP ssp126. Earth System Grid Federation. https://doi.org/10.22033/ESGF/CMIP6.8248
Seland, Ø., Bentsen, M., Oliviè, D. J. L., Toniazzo, T., Gjermundsen, A., Graff, L. S., et al. (2019c). NCC NorESM2-LM model output prepared for CMIP6 ScenarioMIP ssp245. Earth System Grid Federation. https://doi.org/10.22033/ESGF/CMIP6.8253
Seland, Ø., Bentsen, M., Oliviè, D. J. L., Toniazzo, T., Gjermundsen, A., Graff, L. S., et al. (2019d). NCC NorESM2-LM model output prepared for CMIP6 ScenarioMIP ssp585. Earth System Grid Federation. https://doi.org/10.22033/ESGF/CMIP6.8319
Sellar, A. A., Jones, C. G., Mulcahy, J., Tang, Y., Yool, A., Wiltshire, A., et al. (2019). UKESM1: Description and evaluation of the UK Earth System Model. *Journal of Advances in Modeling Earth Systems*, *11*, 4513–4558. https://doi.org/10.1029/2019MS001739
Smeed, D., Moat, B., Rayner, D., Johns, W. E., Baringer, M. O., Volkov, D., & Frajka-Williams, E. (2019). *Atlantic meridional overturning circulation observed by the RAPID-MOCHA-WBTS (RAPID-Meridional Overturning Circulation and Heatflux Array-Western Boundary Time Series) array at 26° N from 2004 to 2018*. UK: British Oceanographic Data Centre - Natural Environment Research Council. https://doi.org/10.5285/8cd7e7bb-9a20-05d8-e053-6c86abc012c2
Steinacher, M., & Joos, F. (2016). Transient Earth system responses to cumulative carbon dioxide emissions: linearities, uncertainties, and probabilities in an observation-constrained model ensemble. *Biogeosciences*, *13*(4), 1071–1103. https://doi.org/10.5194/bg-13-1071-2016
Swart, N. C., Cole, J. N. S., Kharin, V. V., Lazare, M., Scinocca, J. F., Gillett, N. P., et al. (2019a). The Canadian Earth System Model version 5 (CanESM5.0.3). *Geoscientific Model Development*, *12*, 4823–4873. https://doi.org/10.5194/gmd-12-4823-2019
Swart, N. C., Cole, J. N. S., Kharin, V. V., Lazare, M., Scinocca, J. F., Gillett, N. P., et al. (2019b). CCCma CanESM5 model output prepared for CMIP6 CMIP abrupt-4xCO2. Earth System Grid Federation. https://doi.org/10.22033/ESGF/CMIP6.3532
Swart, N. C., Cole, J. N. S., Kharin, V. V., Lazare, M., Scinocca, J. F., Gillett, N. P., et al. (2019c). CCCma CanESM5 model output prepared for CMIP6 CMIP historical. Earth System Grid Federation. https://doi.org/10.22033/ESGF/CMIP6.3610
Swart, N. C., Cole, J. N. S., Kharin, V. V., Lazare, M., Scinocca, J. F., Gillett, N. P., et al. (2019d). CCCma CanESM5 model output prepared for CMIP6 ScenarioMIP ssp126. Earth System Grid Federation. https://doi.org/10.22033/ESGF/CMIP6.3683
Swart, N. C., Cole, J. N. S., Kharin, V. V., Lazare, M., Scinocca, J. F., Gillett, N. P., et al. (2019e). CCCma CanESM5 model output prepared for CMIP6 ScenarioMIP ssp245. Earth System Grid Federation. https://doi.org/10.22033/ESGF/CMIP6.3685
Swart, N. C., Cole, J. N. S., Kharin, V. V., Lazare, M., Scinocca, J. F., Gillett, N. P., et al. (2019f). CCCma CanESM5 model output prepared for CMIP6 ScenarioMIP ssp370. Earth System Grid Federation. https://doi.org/10.22033/ESGF/CMIP6.3690
Swart, N. C., Cole, J. N. S., Kharin, V. V., Lazare, M., Scinocca, J. F., Gillett, N. P., et al. (2019g). CCCma CanESM5 model output prepared for CMIP6 ScenarioMIP ssp585. Earth System Grid Federation. https://doi.org/10.22033/ESGF/CMIP6.3696
Tamsitt, V., Drake, H. F., Morrison, A. K., Talley, L. D., Dufour, C. O., Gray, A. R., et al. (2017). Spiraling pathways of global deep waters to the surface of the Southern Ocean. *Nature Communications*, *8*(1), 172.
Tang, Y., Rumbold, S., Ellis, R., Kelley, D., Mulcahy, J., Sellar, A., & Jones, C. (2019a). MOHC UKESM1.0-LL model output prepared for CMIP6 CMIP abrupt-4xCO2. Earth System Grid Federation. https://doi.org/10.22033/ESGF/CMIP6.5843

Tang, Y., Rumbold, S., Ellis, R., Kelley, D., Mulcahy, J., Sellar, A., et al. (2019b). MOHC UKESM1.0-LL model output prepared for CMIP6 CMIP historical. Earth System Grid Federation. https://doi.org/10.22033/ESGF/CMIP6.6113

Thornalley, D. J., Oppo, D. W., Ortega, P., Robson, J. I., Brierley, C. M., Davis, R., et al. (2018). Anomalously weak Labrador Sea convection and Atlantic overturning during the past 150 years. *Nature*, *556*(7700), 227.

Tomas, R. A., Deser, C., & Sun, L. (2016). The role of ocean heat transport in the global climate response to projected Arctic sea ice loss. *Journal of Climate*, *29*(19), 6841–6859.

Trenberth, K. E., Zhang, Y., Fasullo, J. T., & Cheng, L. (2019). Observation-based estimate of global and basin ocean meridional heat transport time series. *Journal of Climate*, *32*, 4567–4583.

Trossman, D., Palter, J., Merlis, T., Huang, Y., & Xia, Y. (2016). Large-scale ocean circulation-cloud interactions reduce the pace of transient climate change. *Geophysical Research Letters*, *43*, 3935–3943. https://doi.org/10.1002/2016GL067931

Voldoire, A. (2018a). CMIP6 simulations of the CNRM-CERFACS based on CNRM-CM6-1 model for CMIP experiment abrupt-4xCO2. Earth System Grid Federation. https://doi.org/10.22033/ESGF/CMIP6.3916

Voldoire, A. (2018b). CMIP6 simulations of the CNRM-CERFACS based on CNRM-CM6-1 model for CMIP experiment historical. Earth System Grid Federation. https://doi.org/10.22033/ESGF/CMIP6.4066

Voldoire, A. (2019a). CNRM-CERFACS CNRM-CM6-1-HR model output prepared for CMIP6 CMIP abrupt-4xCO2. Earth System Grid Federation. https://doi.org/10.22033/ESGF/CMIP6.3917

Voldoire, A. (2019b). CNRM-CERFACS CNRM-CM6-1-HR model output prepared for CMIP6 CMIP historical. Earth System Grid Federation. https://doi.org/10.22033/ESGF/CMIP6.4067

Voldoire, A. (2019c). CNRM-CERFACS CNRM-CM6-1-HR model output prepared for CMIP6 ScenarioMIP ssp245. Earth System Grid Federation. https://doi.org/10.22033/ESGF/CMIP6.4190

Voldoire, A. (2019d). CNRM-CERFACS CNRM-CM6-1-HR model output prepared for CMIP6 ScenarioMIP ssp585. Earth System Grid Federation. https://doi.org/10.22033/ESGF/CMIP6.4225

Voldoire, A. (2019e). CNRM-CERFACS CNRM-CM6-1 model output prepared for CMIP6 ScenarioMIP ssp126. Earth System Grid Federation. https://doi.org/10.22033/ESGF/CMIP6.4184

Voldoire, A. (2019f). CNRM-CERFACS CNRM-CM6-1 model output prepared for CMIP6 ScenarioMIP ssp245. Earth System Grid Federation. https://doi.org/10.22033/ESGF/CMIP6.4189

Voldoire, A. (2019g). CNRM-CERFACS CNRM-CM6-1 model output prepared for CMIP6 ScenarioMIP ssp370. Earth System Grid Federation. https://doi.org/10.22033/ESGF/CMIP6.4197

Voldoire, A. (2019h). CNRM-CERFACS CNRM-CM6-1 model output prepared for CMIP6 ScenarioMIP ssp585. Earth System Grid Federation. https://doi.org/10.22033/ESGF/CMIP6.4224

Voldoire, A. (2019i). CNRM-CERFACS CNRM-ESM2-1 model output prepared for CMIP6 ScenarioMIP ssp126. Earth System Grid Federation. https://doi.org/10.22033/ESGF/CMIP6.4186

Voldoire, A. (2019j). CNRM-CERFACS CNRM-ESM2-1 model output prepared for CMIP6 ScenarioMIP ssp245. Earth System Grid Federation. https://doi.org/10.22033/ESGF/CMIP6.4191

Voldoire, A. (2019k). CNRM-CERFACS CNRM-ESM2-1 model output prepared for CMIP6 ScenarioMIP ssp370. Earth System Grid Federation. https://doi.org/10.22033/ESGF/CMIP6.4199

Voldoire, A. (2019l). CNRM-CERFACS CNRM-ESM2-1 model output prepared for CMIP6 ScenarioMIP ssp585. Earth System Grid Federation. https://doi.org/10.22033/ESGF/CMIP6.4226

Voldoire, A., Saint-Martin, D., Sénési, S., Decharme, B., Alias, A., Chevallier, M., et al. (2019). Evaluation of CMIP6 DECK experiments with CNRM-CM6-1. *Journal of Advances in Modeling Earth Systems*, *11*, 2177–2213. https://doi.org/10.1029/2019MS001683

Volodin, E., Mortikov, E., Gritsun, A., Lykossov, V., Galin, V., Diansky, N., & Emelina, S. (2019a). INM INM-CM4-8 model output prepared for CMIP6 CMIP abrupt-4xCO2. Earth System Grid Federation. https://doi.org/10.22033/ESGF/CMIP6.4931

Volodin, E., Mortikov, E., Gritsun, A., Lykossov, V., Galin, V., Diansky, N., & Emelina, S. (2019b). INM INM-CM4-8 model output prepared for CMIP6 CMIP historical. Earth System Grid Federation. https://doi.org/10.22033/ESGF/CMIP6.5069

Volodin, E., Mortikov, E., Gritsun, A., Lykossov, V., Galin, V., Diansky, N., & Emelina, S. (2019c). INM INM-CM4-8 model output prepared for CMIP6 ScenarioMIP ssp126. Earth System Grid Federation. https://doi.org/10.22033/ESGF/CMIP6.12325

Volodin, E., Mortikov, E., Gritsun, A., Lykossov, V., Galin, V., Diansky, N., & Emelina, S. (2019d). INM INM-CM4-8 model output prepared for CMIP6 ScenarioMIP ssp245. Earth System Grid Federation. https://doi.org/10.22033/ESGF/CMIP6.12327

Volodin, E., Mortikov, E., Gritsun, A., Lykossov, V., Galin, V., Diansky, N., & Emelina, S. (2019e). INM INM-CM4-8 model output prepared for CMIP6 ScenarioMIP ssp370. Earth System Grid Federation. https://doi.org/10.22033/ESGF/CMIP6.12329

Volodin, E., Mortikov, E., Gritsun, A., Lykossov, V., Galin, V., Diansky, N., & Emelina, S. (2019f). INM INM-CM4-8 model output prepared for CMIP6 ScenarioMIP ssp585. Earth System Grid Federation. https://doi.org/10.22033/ESGF/CMIP6.12337

Volodin, E., Mortikov, E., Gritsun, A., Lykossov, V., Galin, V., Diansky, N., & Emelina, S. (2019g). INM INM-CM5-0 model output prepared for CMIP6 CMIP abrupt-4xCO2. Earth System Grid Federation. https://doi.org/10.22033/ESGF/CMIP6.4932

Volodin, E., Mortikov, E., Gritsun, A., Lykossov, V., Galin, V., Diansky, N., & Emelina, S. (2019h). INM INM-CM5-0 model output prepared for CMIP6 CMIP historical. Earth System Grid Federation. https://doi.org/10.22033/ESGF/CMIP6.5070

Volodin, E., Mortikov, E., Gritsun, A., Lykossov, V., Galin, V., Diansky, N., & Emelina, S. (2019i). INM INM-CM5-0 model output prepared for CMIP6 ScenarioMIP ssp126. Earth System Grid Federation. https://doi.org/10.22033/ESGF/CMIP6.12326

Volodin, E., Mortikov, E., Gritsun, A., Lykossov, V., Galin, V., Diansky, N., & Emelina, S. (2019j). INM INM-CM5-0 model output prepared for CMIP6 ScenarioMIP ssp245. Earth System Grid Federation. https://doi.org/10.22033/ESGF/CMIP6.12328

Volodin, E., Mortikov, E., Gritsun, A., Lykossov, V., Galin, V., Diansky, N., & Emelina, S. (2019k). INM INM-CM5-0 model output prepared for CMIP6 ScenarioMIP ssp370. Earth System Grid Federation. https://doi.org/10.22033/ESGF/CMIP6.12330

Volodin, E., Mortikov, E., Gritsun, A., Lykossov, V., Galin, V., Diansky, N., & Emelina, S. (2019l). INM INM-CM5-0 model output prepared for CMIP6 ScenarioMIP ssp585. Earth System Grid Federation. https://doi.org/10.22033/ESGF/CMIP6.12338

Volodin, E., Mortikov, E., Kostrykin, S., Galin, V. Y., Lykossov, V., Gritsun, A., et al. (2017). Simulation of the present-day climate with the climate model INMCM5. *Climate Dynamics*, *49*(11-12), 3715–3734.

Volodin, E. M., Mortikov, E. V., Kostrykin, S. V., Galin, V. Y., Lykossov, V. N., Gritsun, A. S., et al. (2018). Simulation of the modern climate using the INM-CM48 climate model. *Russian Journal of Numerical Analysis and Mathematical Modelling*, *33*(6), 367–374.

Weaver, A. J., Sedláček, J., Eby, M., Alexander, K., Crespin, E., Fichefet, T., et al. (2012). Stability of the Atlantic meridional overturning circulation: A model intercomparison. *Geophysical Research Letters*, *39*.

Wieners, K. H., Giorgetta, M., Jungclaus, J., Reick, C., Esch, M., Bittner, M., & Roeckner, E. (2019a). MPI-M MPI-ESM1.2-LR model output prepared for CMIP6 CMIP historical. Earth System Grid Federation. https://doi.org/10.22033/ESGF/CMIP6.6595

Wieners, K. H., Giorgetta, M., Jungclaus, J., Reick, C., Esch, M., Bittner, M., & Roeckner, E. (2019b). MPI-M MPI-ESM1.2-LR model output prepared for CMIP6 ScenarioMIP ssp126. Earth System Grid Federation. https://doi.org/10.22033/ESGF/CMIP6.6690
Wieners, K. H., Giorgetta, M., Jungclaus, J., Reick, C., Esch, M., Bittner, M., & Roeckner, E. (2019c). MPI-M MPI-ESM1.2-LR model output prepared for CMIP6 ScenarioMIP ssp245. Earth System Grid Federation. https://doi.org/10.22033/ESGF/CMIP6.6693
Wieners, K. H., Giorgetta, M., Jungclaus, J., Reick, C., Esch, M., Bittner, M., & Roeckner, E. (2019d). MPI-M MPI-ESM1.2-LR model output prepared for CMIP6 ScenarioMIP ssp370. Earth System Grid Federation. https://doi.org/10.22033/ESGF/CMIP6.6695
Wieners, K. H., Giorgetta, M., Jungclaus, J., Reick, C., Esch, M., Bittner, M., & Roeckner, E. (2019e). MPI-M MPI-ESM1.2-LR model output prepared for CMIP6 ScenarioMIP ssp585. Earth System Grid Federation. https://doi.org/10.22033/ESGF/CMIP6.6705
Williams, K., Copsey, D., Blockley, E., Bodas-Salcedo, A., Calvert, D., Comer, R., et al. (2018). The Met Office global coupled model 3.0 and 3.1 (GC3. 0 and GC3. 1) configurations. *Journal of Advances in Modeling Earth Systems*, *10*, 357–380. https://doi.org/10.1002/2017MS001115
Winton, M., Adcroft, A., Griffies, S. M., Hallberg, R. W., Horowitz, L. W., & Stouffer, R. J. (2013). Influence of ocean and atmosphere components on simulated climate sensitivities. *Journal of Climate*, *26*(1), 231–245.
Winton, M., Anderson, W. G., Delworth, T. L., Griffies, S. M., Hurlin, W. J., & Rosati, A. (2014). Has coarse ocean resolution biased simulations of transient climate sensitivity? *Geophysical Research Letters*, *41*, 8522–8529. https://doi.org/10.1002/2014GL061523
Yeager, S., & Robson, J. (2017). Recent progress in understanding and predicting Atlantic decadal climate variability. *Current Climate Change Reports*, *3*(2), 112–127.
Yu, Y. (2019a). CAS FGOALS-f3-L model output prepared for CMIP6 CMIP abrupt-4xCO2. Earth System Grid Federation. https://doi.org/10.22033/ESGF/CMIP6.3176
Yu, Y. (2019b). CAS FGOALS-f3-L model output prepared for CMIP6 CMIP historical. Earth System Grid Federation. https://doi.org/10.22033/ESGF/CMIP6.3355
Yu, Y. (2019c). CAS FGOALS-f3-L model output prepared for CMIP6 ScenarioMIP ssp126. Earth System Grid Federation. https://doi.org/10.22033/ESGF/CMIP6.3464
Yu, Y. (2019d). CAS FGOALS-f3-L model output prepared for CMIP6 ScenarioMIP ssp245. Earth System Grid Federation. https://doi.org/10.22033/ESGF/CMIP6.3468
Yu, Y. (2019e). CAS FGOALS-f3-L model output prepared for CMIP6 ScenarioMIP ssp370. Earth System Grid Federation. https://doi.org/10.22033/ESGF/CMIP6.3479
Yu, Y. (2019f). CAS FGOALS-f3-L model output prepared for CMIP6 ScenarioMIP ssp585. Earth System Grid Federation. https://doi.org/10.22033/ESGF/CMIP6.3502
Yukimoto, S., Kawai, H., Koshiro, T., Oshima, N., Yoshida, K., Urakawa, S., et al. (2019). The meteorological research institute Earth system model Version 2.0, MRI-ESM2. 0: Description and basic evaluation of the physical component. *Journal of the Meteorological Society of Japan. Ser. II*, 98. https://doi.org/10.2151/jmsj.2019-051
Yukimoto, S., Koshiro, T., Kawai, H., Oshima, N., Yoshida, K., Urakawa, S., & Adachi, Y. (2019a). MRI MRI-ESM2.0 model output prepared for CMIP6 CMIP abrupt-4xCO2. Earth System Grid Federation. https://doi.org/10.22033/ESGF/CMIP6.6755
Yukimoto, S., Koshiro, T., Kawai, H., Oshima, N., Yoshida, K., Urakawa, S., & Adachi, Y. (2019b). MRI MRI-ESM2.0 model output prepared for CMIP6 CMIP historical. Earth System Grid Federation. https://doi.org/10.22033/ESGF/CMIP6.6842
Zelinka, M. D., Myers, T. A., McCoy, D. T., Po-Chedley, S., Caldwell, P. M., Ceppi, P., et al. (2020). Causes of higher climate sensitivity in CMIP6 models. *Geophysical Research Letters*, *47*, e85782. https://doi.org/10.1029/2019GL085782
Ziehn, T., Chamberlain, M., Lenton, A., Law, R., Bodman, R., Dix, M., & Druken, K. (2019a). CSIRO ACCESS-ESM1.5 model output prepared for CMIP6 CMIP abrupt-4xCO2. Earth System Grid Federation. https://doi.org/10.22033/ESGF/CMIP6.4238
Ziehn, T., Chamberlain, M., Lenton, A., Law, R., Bodman, R., Dix, M., & Druken, K. (2019b). CSIRO ACCESS-ESM1.5 model output prepared for CMIP6 CMIP historical. Earth System Grid Federation. https://doi.org/10.22033/ESGF/CMIP6.4272
Ziehn, T., Chamberlain, M., Lenton, A., Law, R., Bodman, R., Dix, M., & Druken, K. (2019c). CSIRO ACCESS-ESM1.5 model output prepared for CMIP6 ScenarioMIP ssp126. Earth System Grid Federation. https://doi.org/10.22033/ESGF/CMIP6.4320
Ziehn, T., Chamberlain, M., Lenton, A., Law, R., Bodman, R., Dix, M., & Druken, K. (2019d). CSIRO ACCESS-ESM1.5 model output prepared for CMIP6 ScenarioMIP ssp245. Earth System Grid Federation. https://doi.org/10.22033/ESGF/CMIP6.4322
Ziehn, T., Chamberlain, M., Lenton, A., Law, R., Bodman, R., Dix, M., & Druken, K. (2019e). CSIRO ACCESS-ESM1.5 model output prepared for CMIP6 ScenarioMIP ssp370. Earth System Grid Federation. https://doi.org/10.22033/ESGF/CMIP6.4324
Ziehn, T., Chamberlain, M., Lenton, A., Law, R., Bodman, R., Dix, M., & Druken, K. (2019f). CSIRO ACCESS-ESM1.5 model output prepared for CMIP6 ScenarioMIP ssp585. Earth System Grid Federation. https://doi.org/10.22033/ESGF/CMIP6.4333
Ziehn, T., Lenton, A., Law, R. M., Matear, R. J., & Chamberlain, M. A. (2017). The carbon cycle in the Australian Community Climate and Earth System Simulator (ACCESS-ESM1)—Part 2: Historical simulations. *Geoscientific Model Development*, *10*(7).

References From the Supporting Information

Pedregosa, F., Varoquaux, G., Gramfort, A., Michel, V., Thirion, B., Grisel, O., et al. (2011). Scikit-learn: Machine learning in python. *Journal of Machine Learning Research*, *12*, 2825–2830.